Chemical Science

ROYAL SOCIETY OF CHEMISTRY

EDGE ARTICLE

View Article Online
View Journal | View Issue

Check for updates

Cite this: *Chem. Sci.*, 2024, **15**, 11657

All publication charges for this article have been paid for by the Royal Society of Chemistry

Received 3rd June 2024
Accepted 21st June 2024

DOI: 10.1039/d4sc03629h

rsc.li/chemical-science

Open Access Article. Published on 28 June 2024. Downloaded on 1/18/2026 3:16:03 PM. This article is licensed under a Creative Commons Attribution-NonCommercial 3.0 Unported Licence.

In situ bioorthogonal-modulation of m^{6}A RNA methylation in macrophages for efficient eradication of intracellular bacteria†

Mengyu Sun,[ab] Jinsong Ren *[ab] and Xiaogang Qu *[ab]

N^6-Methyladenosine (m^{6}A) methylation plays a critical role in controlling the RNA fate. Emerging evidence has demonstrated that aberrant m^{6}A methylation in immune cells such as macrophages could alter cell homeostasis and function, which can be a promising target for disease treatment. Despite tremendous progress in regulating the level of m^{6}A methylation, the current methods suffer from the time-consuming operation and annoying off-target effect, which hampers the *in situ* manipulation of m^{6}A methylation. Here, a bioorthogonal *in situ* modulation strategy of m^{6}A methylation was proposed. Well-designed covalent organic framework (COF) dots (CIDM) could deprotect the agonist prodrug of m^{6}A methyltransferase, resulting in a considerable hypermethylation of m^{6}A modification. Simultaneously, the bioorthogonal catalyst CIDM showed oxidase (OXD)-mimic activity that further promoted the level of m^{6}A methylation. Ultimately, the potential therapeutic effect of bioorthogonal controllable regulation of m^{6}A methylation was demonstrated through intracellular bacteria eradication. The remarkable antimicrobial outcomes indicate that upregulating m^{6}A methylation in macrophages could reprogram them into the M1 phenotype with high bactericidal activity. We believe that our bioorthogonal chemistry-controlled epigenetics regulatory strategy will provide a unique insight into the development of controllable m^{6}A methylation.

Introduction

As the most prevalent and important chemical modification in eukaryotes, the N^6-methyladenosine (m^{6}A) mRNA methylation has drawn considerable attention. It is prominent for most biological processes such as circadian rhythm,[1] embryonic development,[2] cancer progression[3–8] and stem cell self-renewal.[9–11] Notably, compelling evidence suggests that m^{6}A methylation has critical functions in the maintenance of immune cell homeostasis and function.[12–14] As an essential component of the innate immune system, the phenotype and dysfunction of macrophages are regulated by m^{6}A methylation. For instance, a low level of m^{6}A methylation by deletion of METTL3 has been reported to attenuate the antitumor ability *via* influencing macrophage reprogramming.[15] Besides, research validates that the disorder of m^{6}A methylation in macrophages by depleting METTL3 can depress their competence to defend against pathogens.[16] Additionally, the studies of Cao's group have implicated that inhibiting the demethylation of m^{6}A in macrophages by deleting demethylase alkB homolog 5 (ALKBH5) can inhibit viral replication.[17] In light of these, the modulation of m^{6}A methylation can be a promising therapeutic strategy for disease treatment.[18] Despite tremendous efforts devoted to modulating m^{6}A methylation, some thorny challenges still need to be tackled. For example, classical genetic approaches such as knockouts/downs and mutations[19–21] are time-consuming to operate and costly to manufacture. Alternatively, the utilization of small molecule agents serves as a common method to regulate m^{6}A methylation.[22–25] Nevertheless, it is often flawed in off-target and random distribution, resulting in side effects. Although the light-controllable chemical method holds the potential to modulate hypermethylation of m^{6}A,[26–28] the inevitable phototoxicity and the shallow tissue penetration depths impose additional obstacles to its application in clinics. Therefore, it's urgent to develop an efficient and convenient approach to *in situ* manipulate m^{6}A methylation in physiological environments.

Bioorthogonal chemistry has emerged as a booming technique for manipulating complicated biological processes in the native environment, stimulating a wide range of research interests.[29–31] Given its merit of high selectivity, outstanding efficiency and solid reliability, this powerful tool has been widely used in complex biological conditions. For example, the applications of bioorthogonal reactions in living systems revolutionize the technique to label and manipulate intact

[a]*Laboratory of Chemical Biology and State Key Laboratory of Rare Earth Resource Utilization, Changchun Institute of Applied Chemistry, Chinese Academy of Sciences, Changchun, Jilin 130022, China. E-mail: jren@ciac.ac.cn; xqu@ciac.ac.cn*

[b]*University of Science and Technology of China, Hefei, Anhui, 230029, China*

† Electronic supplementary information (ESI) available. See DOI: https://doi.org/10.1039/d4sc03629h

© 2024 The Author(s). Published by the Royal Society of Chemistry

Open Access Article. Published on 28 June 2024. Downloaded on 1/18/2026 3:16:03 PM. This article is licensed under a Creative Commons Attribution-NonCommercial 3.0 Unported Licence.

biomolecules of glycosylation, protein biophysics and other life processes.[32–38] In addition, some bioorthogonal cleavage reactions have been developed for protein activation in their native habitats, which offered a spatiotemporally controlled protein activation strategy.[39–42] Recently, bioorthogonal reactions have been garnering considerable attention in therapeutic applications by generating imaging and therapeutic agents *in situ*.[43–48] The bioorthogonal activation of prodrugs controls the generation of therapeutics in a locally constrained manner, which avoids the traditional adverse effect of drugs. Collectively, coupled with the features of controllable manner and minimal adverse reactions, the bioorthogonal chemistry is feasible to serve as an excellent candidate for *in situ* modulating RNA modification.

Keep this in mind, herein we proposed a bioorthogonal regulation strategy for m^{6}A methylation (Scheme 1). In our design, the bioorthogonal catalysis system (CIDM) was composed of ferric porphyrin-based COF dots and modified with mannose for targeting macrophages and synthesizing prodrugs. This well-designed CIDM possessed ultrasmall size and increased specific surface area, which enabled it to penetrate easily and catalyze effectively. The parent drug piperidine-3-carboxylate (MPCH), which is an agonist of m^{6}A writer protein, methyltransferase-like 3 (METTL3)/methyltransferase-like 14 (METTL14) complex protein,[26,49] was chosen as a model drug to mask with the aryl azide carbonate group. The activity of pro-MPCH was rapidly *in situ* restored by CDM nanocatalysts, resulting in a considerable hypermethylation of m^{6}A modification in transcriptome RNAs. Interestingly, the constructed CIDM displayed OXD-mimic activity, which could facilitate the modulation of m^{6}A methylation.[50–52] As a proof of concept, we applied this strategy to reprogram macrophage polarization into the bactericidal M1 phenotype for efficient bacterial ablation.[15,16,53,54] Such a bioorthogonal chemistry-controlled epigenetics regulatory strategy could achieve a maximized treatment outcome and a minimized drug side effect, which provided an important insight into the development of *in situ* controllable m^{6}A methylation.

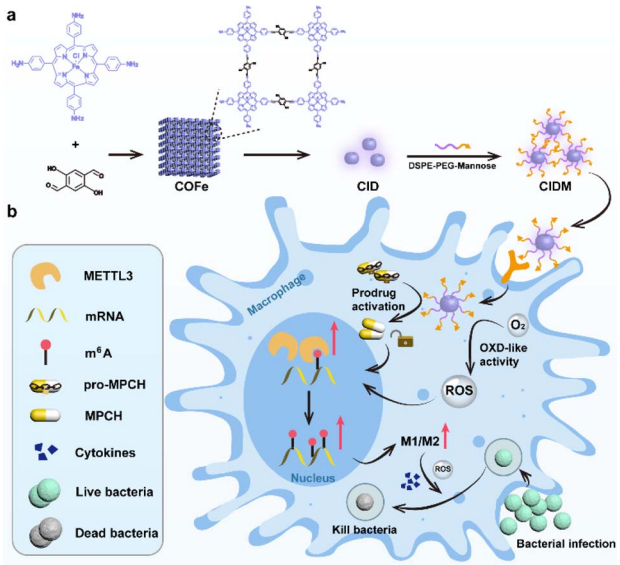

Scheme 1 (a) Schematic representation of the formation of CIDM. (b) Schematic illustration of CIDM for regulation of m^{6}A methylation in macrophages by bioorthogonal catalysis prodrug activation and generation of ROS, which can reprogram macrophages into the M1-type and eradicate pathogenic bacteria.

Results and discussion

To validate our protocol, the nanocatalyst CIDM was synthesized through three steps. At first, COFe was synthesized based on our previous report.[47] The Fourier transform infrared (FTIR) results confirmed the successful synthesis of COFe, as evidenced by the disappearance of N–H stretching bonds (3357 cm^{-1}) and the formation of C=O stretching bonds (1606 cm^{-1}) (Fig. 1a).[55] Besides, the existence of the Fe element in synthesized COFe was confirmed by energy-dispersive spectroscopy (EDS, Fig. S1†). Subsequently, the COF nanodots were prepared by ultrasonic dispersion. As illustrated in Scheme 1a, the strategy consisting of water bath sonication and ultrasound probe sonication was utilized to exfoliate bulk COFe (denoted as CID). X-ray photoelectron spectroscopy (XPS) was carried out to analyze the mechanism of the structural transformation. Fig. S2† shows the N 1s outcome of CID. The peak at 398.54 eV was related to the four N atoms coordinated to the central Fe. The component located at 400.05 eV was consistent with pyrrolic groups. The spectrum of CID showed the nitrogen in proton NH^{3+} (401.65 eV).[56,57] It was supposed that most of the relatively unstable hemiaminal structures and part of the imine bonds in COFe were fractured into NH^{3+} by ultrasonic waves. Furthermore, the FITR spectra of CID showed the stretching bands of N–H at 3357 cm^{-1} and C=O at 1606 cm^{-1}, also proving that the imine bonds partly fractured into NH^{3+} (Fig. 1a). Afterward, to enhance the application of the CID nanocatalyst in

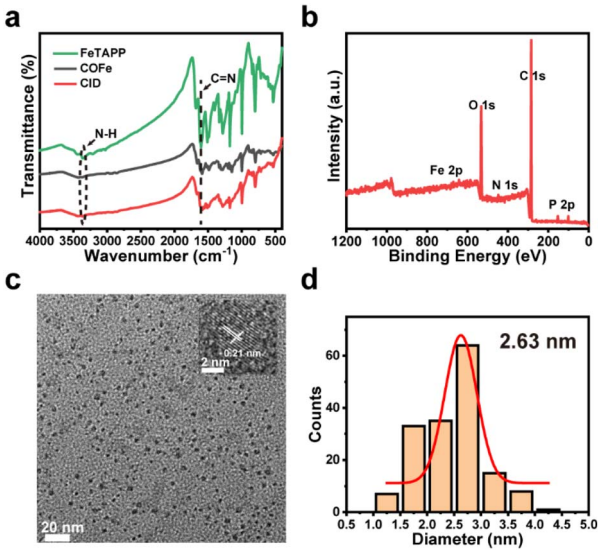

Fig. 1 (a) FTIR spectra of FeTAPP, COFe and CID. (b) XPS analysis of CIDM. (c) TEM image of CIDM. Inset: image of individual CIDM. (d) Diameter distribution measured from the TEM image of CIDM.

© 2024 The Author(s). Published by the Royal Society of Chemistry

Open Access Article. Published on 28 June 2024. Downloaded on 1/18/2026 3:16:03 PM. This article is licensed under a Creative Commons Attribution-NonCommercial 3.0 Unported Licence.

physiological environments, poly(ethylene glycol) (PEG)-mannose was further employed to decorate the surface of the COF nanocatalyst (denoted as CIDM NCs). The P element appeared in the XPS spectrum of CIDM, suggesting that the modification with DSPE-PEG-mannose was successful (Fig. 1b). In addition, transmission electron microscopy (TEM) was further utilized to characterize CIDM (Fig. 1c). The CIDM showed average sizes of 2.63 nm as observed under the TEM image (Fig. 1d). Thanks to the modification with PEG, the CIDM nanocatalyst displayed complete dispersion and good stabilization in different physiological solutions (Fig. S3†). After dispersing in phosphate buffered saline (PBS, 10 mM), Dulbecco's modified Eagle medium (DMEM) and fetal bovine serum (FBS) for 24 h, the CIDM exhibited high stability without agglomeration.

Motivated by the successful synthesis of CIDM, we investigated its catalytical performance. In the first place, the reaction of de-caging the rhodamine 110 derivative (pro-RH 110) was carried out to evaluate the ability of CIDM to catalyze bioorthogonal reactions (Fig. 2a, S4 and S30†). The synthesis of the azide bond effectively quenched the fluorescence of rhodamine 110, enabling the monitoring of the deprotection reaction triggered by the CIDM nanocatalyst.[58] Fig. S5† shows that pro-RH 110 alone had almost no fluorescence. Upon the addition of CIDM to pro-RH 110 for 24 h, the sample emitted green fluorescence, indicating that RH 110 was produced (Fig. S6†). Next, we investigated the differences in catalytic performance among CID, CIDM and bulk COFe (Fig S7†). As expected, there was no obvious difference in catalytic activity between CID and CIDM, reflecting that the modification with PEG and mannose did not affect the catalytic activity. Surprisingly, the catalytic activity of the CID was higher compared to bulk COFe. We attributed this to the ultrasmall size and increased specific surface area of the CID nanocatalyst. These admirable characteristics enable it to increase electron transfer and expose more active sites, which accelerates the catalytic performance. Further, CIDM exhibited brilliant bioorthogonal catalytic activity in a dose-dependent manner according to the change of fluorescence intensity at 530 nm (Fig. S8†). To determine the catalytic efficiency and the kinetic process of CIDM, we recorded the changes in the fluorescence spectrum of pro-RH 110 treated with the catalysts. The results confirmed that the fluorescence of RH 110 gradually increased over time with the help of the CIDM catalyst (Fig. 2b–d). Moreover, the catalytic performance of CIDM remained good under different reaction conditions (Fig. S9†). Overall, the above results confirmed that the designed CIDM possessed remarkable catalytic performance, laying the foundation for subsequent research on intracellular prodrug activation and m^{6}A methylation modulation.

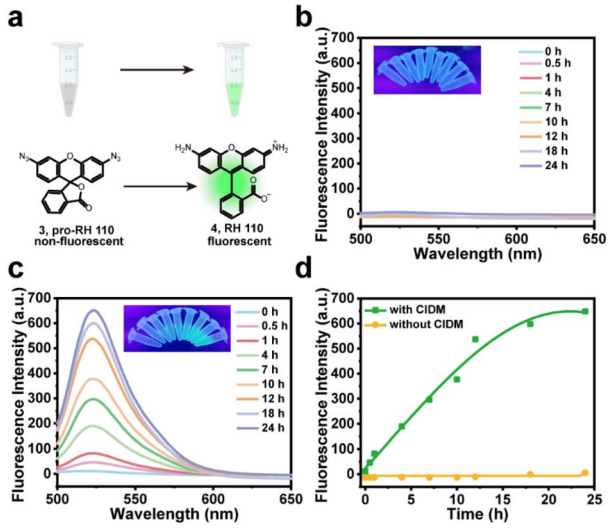

Fig. 2 (a) Schematic representation of deprotection catalyzed by CIDM. Fluorescence spectra at different times (0–24 h) of (b) pro-RH 110 + NaAsc and (c) pro-RH 110 + CIDM + NaAsc, and the related photograph of the reaction is in the inset of the figure. (d) Fluorescence intensity of the released RH 110 at different times (0–24 h). With CIDM, groups (green line) are CIDM + pro-RH 110 + NaAsc. Without CIDM, groups (orange line) are pro-RH 110 + NaAsc. Experimental conditions: CIDM (50 μg mL^{-1}), pro-RH 110 (10 μM) and 5 mM NaAsc. RH 110 (λ_{ex} = 488 nm, λ_{em} = 530 nm).

Having confirmed the bioorthogonal catalytic capability of CIDM, we further explored the intracellular behaviors by using the RAW264.7 (mouse leukemia cells of monocyte macrophages) cell as a model cell. As a premise, the quantitative detection of uptake rates between COFe, CID and CIDM was performed by confocal laser scanning microscopy (CLSM) and flow cytometry. According to Fig. S10,† CID with ultrasmall size penetrated cells more easily than bulk COFe. In addition, confocal images showed that the uptake of CIDM with mannose modification by the macrophages was more efficient in contrast to CID (Fig. S10†).[59] Besides, a similar trend was observed in the quantitative detection of uptake rates using flow cytometry (Fig. S11†). Subsequently, the methyl thiazolyl tetrazolium (MTT) assay was carried out to measure the cytotoxicity of CIDM. Fig. S12† reveals that CIDM exhibited good biocompatibility, as more than 80% of RAW264.7 cells maintained vitality at a concentration of 200 μg mL^{-1} after 48 h. Following that, we examined the catalytic ability of CIDM to activate the cleavage reaction by using rhodamine 110 (RH 110) as a substrate (Fig. 3a). Fluorescence images showed that the cells incubated with CIDM + pro-RH 110 exhibited stronger green fluorescence, while little to no fluorescence was observed in control groups (Fig. 3c and S13†). In addition, the flow cytometric analysis was consistent with the fluorescence imaging result (Fig. 3b and d). The mean fluorescence intensity (MFI) in Fig. 3d showed that the fluorescence intensity of the CIDM + pro-RH 110 group was 5.2-fold higher than that of the pro-RH 110 group. These results proved the remarkable catalytic performance of CIDM *in vitro*. Overall, CIDM NCs not only exhibited excellent targeting ability to macrophages, but also owned the characteristic of catalytic ability.

Based on the admirable qualities of CIDM, the deprotection capability of CIDM NCs to activate prodrugs was explored. It is reported that the piperidine ring from piperidine-3-carboxylate (MPCH) could arise from multiple cooperative interactions with m^{6}A writer METTL3/14 complex protein, thus serving as an agonist for m^{6}A methylation regulation.[49] In the following, we chose MPCH as a model drug and synthesized the MPCH

Open Access Article. Published on 28 June 2024. Downloaded on 1/18/2026 3:16:03 PM.
This article is licensed under a Creative Commons Attribution-NonCommercial 3.0 Unported Licence.

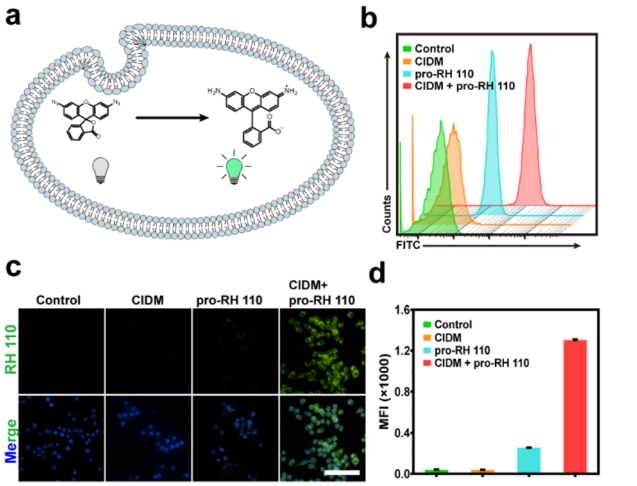

Fig. 3 (a) Schematic representation of the CIDM-mediated cleavage reaction in RAW264.7 macrophage cells. The flow cytometry analysis of (b) fluorescence changes and (d) MFI after different treatments. Data are presented as mean ± s.d. (n = 3). (c) The fluorescence images of RAW264.7 cells after various treatments. Scale bar = 50 μm. The nuclei are stained by DAPI. The quantitative analysis of (c) is shown in Fig. S13.† RAW264.7 cells are pre-incubated with CIDM (50 μg mL^{-1}) for 12 h, then incubated with a medium containing pro-RH 110 (20 μM) and 5 mM NaAsc for another 12 h. Data are presented as mean ± s.d. (n = 3). ****p < 0.0001.

prodrug (pro-MPCH) by blocking the functional N–H group on MPCH with an aryl azide carbonate unit (Fig. S31 and S32†).[58,60] At first, mass spectrometry (MS) was used to detect the intracellular activation of MPCH by CIDM NCs. Fig. S14B† confirms that pro-MPCH was de-caged with the catalysis of CIDM. Then, the MTT assay was carried out to determine that the activated drugs did not affect the cell growth of RAW264.7 cells (Fig. S15†). Subsequently, to determine the function of activated pro-MPCH, the m^{6}A methylation in macrophages treated with CIDM NCs and pro-MPCH was measured by RNA dot blot analysis. As shown in Fig. 4a and b, the pro-MPCH treated group almost did not affect m^{6}A methylation in contrast to the control group. This phenomenon showed that the masking group completely covered the function of MPCH. It was worth noting that the RAW264.7 cells treated with pro-MPCH + CIDM NCs performed the highest level of m^{6}A methylation, even higher than the MPCH-treated group. Additionally, the m^{6}A modification level was further investigated by the ELISA assay (Fig. S16†). There was no doubt that the RAW264.7 cells showed a significant increase in the m^{6}A modification level after stimulation with pro-MPCH + CIDM NCs. Surprisingly, we noticed that the m^{6}A modification level was elevated in the presence of CIDM compared to the PBS-treated group. Research demonstrated that reactive oxygen species (ROS) could significantly induce m^{6}A levels.[50–52] To determine the ability of CIDM to generate ROS, we observed the change of absorption at 652 nm in the presence of the substrate 3,3′,5,5′-tetramethylbenzidine (TMB). The absorption increased after the addition of CIDM, proving that CIDM possessed the activity to produce ROS (Fig. S17†). This phenomenon further implies that CIDM NCs with OXD-mimic properties could modulate m^{6}A methylation to a certain degree. Meanwhile, the activity of CIDM increased rapidly with increasing concentration (Fig. S18†). Besides, as shown in Fig. S19–S21,† the enzyme-like activity was dependent on pH, temperature, and TMB concentration. Next, to investigate the OXD-mimic properties of CIDM in living cells, the intracellular ROS was measured using a 2,7-dichlorodihydrofluorescein diacetate (DCFH-DA) probe, which would be oxidized to 2,7-dichlorofluorescein (DCF) with strong green fluorescence. Fig. S22† depicts that the green fluorescence in CIDM-treated RAW264.7 cells increased in a concentration-dependent manner, demonstrating that the OXD-like activity of CIDM could generate ROS in RAW264.7 cells. Together, all these data confirmed our strategy that the masked agonist pro-MPCH could be revivified to modulate m^{6}A methylation through the CIDM NC catalyzed biorthogonal cleavage reaction. Meanwhile, CIDM NCs with OXD-mimic activity could generate ROS. The generation of ROS and the activated drug synergistically promoted the hypermethylation of m^{6}A modification.

Next, we investigated the effect of elevated m^{6}A methylation on macrophage polarization into the M1 phenotype.[15,16] The expression of surface biomarkers and the secretion of cell cytokines in the treated macrophages were detected by flow cytometry analysis, qPCR assay and ELISA assay, respectively (Fig. 4c and d). During the experiment, the RAW264.7 cells were reshaped into the M2 phenotype by IL-4.[61] As is well known, the upregulation of CD86 served as a surface biomarker for M1-type macrophages, while the upregulation of CD206 served as a surface biomarker for M2-type macrophages. As depicted in Fig. 4d, the populations of CD206 and CD86 on RAW264.7 cells from the pro-MPCH treated group were almost consistent with the group only treated with PBS. Post-treatment with CIDM NCs, the population of CD206 on macrophages decreased and CD86 increased in contrast to the control group. These results are attributed to the production of ROS, which promoted the phenotypic polarization of macrophages by inducing upregulation of m^{6}A methylation. Notably, the expression of CD206 in the CIDM NCs + pro-MPCH treated group was most down-regulated, while the expression of CD86 was extremely promoted. The CD86 biomarker in the CIDM NCs + pro-MPCH treated group was approximately 58.8%, which was 4.63-fold higher than that of the prodrug-treated group. In addition, the qPCR assay was executed to evaluate the secreting levels of cytokines including Arg I, IL-10 and iNOS, TNF-α, corresponding to M2 phenotypic related genes and M1 phenotypic related genes (Fig. 4c). After pretreating macrophages with IL-4, the CIDM NCs combined with the pro-MPCH group showed a significantly increased level of iNOS and TNF-α secretion. Meanwhile, the levels of Arg I and IL-10 decreased compared to the other groups. Furthermore, ELISA assays were conducted to test the generation levels of M1 markers IL-6 and IL-1β. Fig. S23† illustrates that the IL-6 and IL-1β secretion elevated significantly after CIDM NCs + pro-MPCH stimulation. All of the above evidence demonstrated that post treatment with CIDM NCs and pro-MPCH, the macrophages could re-differentiate into the M1 phenotype through the *in situ* restoration of MPCH combined with the production of ROS. Since the m^{6}A

© 2024 The Author(s). Published by the Royal Society of Chemistry

Open Access Article. Published on 28 June 2024. Downloaded on 1/18/2026 3:16:03 PM. This article is licensed under a Creative Commons Attribution-NonCommercial 3.0 Unported Licence.

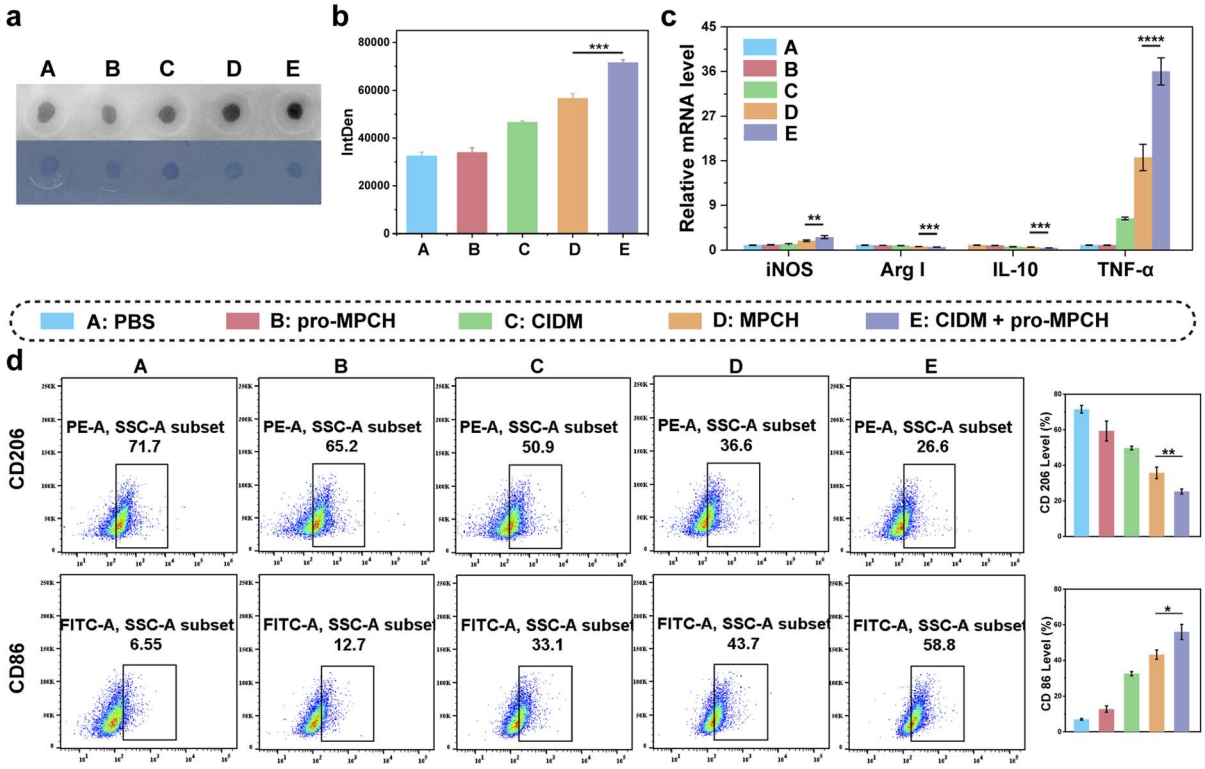

Fig. 4 (a) Determination of m^{6}A abundance in RAW264.7 cells and (b) the gray value analysis after various treatments by the dot blot assay. (c) Relative mRNA level of M1-related genes (iNOS and TNF-α) and M2-related genes (Arg I and IL-10) measured by real-time qPCR. Data are presented as mean ± s.d. ($n = 3$). (d) Flow cytometry analysis of the proportion of CD206 and CD86 in macrophages after different treatments. RAW264.7 cells were pre-incubated with IL-4 (25 ng mL^{-1}) for 12 h and then divided into five groups: A: PBS, B: pro-MPCH, C: CIDM, D: MPCH and E: CIDM + pro-MPCH. Experimental conditions: CIDM (50 μg mL^{-1}), pro-MPCH (100 nM), 5 mM NaAsc. Data are presented as mean ± s.d. ($n = 3$). *P < 0.05, **P < 0.01.

enhancement potentiated M1-type macrophages, we further determined the factor driving the polarization of macrophages. The expression level of STAT1 was measured by qPCR, where STAT1 is one of the major transcriptional regulators of M1 macrophage polarization.[15,62] Fig. S24† shows that the treatment with CIDM and pro-MPCH markedly increased the expression of STAT1 mRNA. Furthermore, the upregulation of m^{6}A methylation greatly increased the expression of STAT1 protein as well (Fig. S25†), indicating that bioorthogonally modulated m^{6}A mainly affected the mRNA levels of STAT1 to further upregulate protein levels. In a word, these results suggested that M1 macrophages might be polarized by the upregulation of STAT1 mRNA and STAT1 protein.

Given the potent ability of CIDM NCs to polarize macrophages, we verified the bactericidal ability of repolarized M1-type macrophages. As reported in the literature, M1 macrophages can efficiently eradicate pathogenic bacteria through phagocytosis and killing actions.[16,53,54,63] To determine the effect of different treatments on the phagocytosis of macrophages, a common reagent, the neutral red reagent was used to test the phagocytic function of macrophages.[61] Fig. S26† shows the absorption at 540 nm of macrophages after various treatments. The absorption of group E treated with CIDM NCs + pro-MPCH was the highest compared to the other groups, indicating the enhanced phagocytosis of treated macrophages. Then, we determined the effect of different manipulations on the phagocytosis of Methicillin-resistant *Staphylococcus aureus* (MRSA) by RAW264.7 macrophages by CLSM and flow cytometry (Fig. 5a–c). Fluorescence co-localization images displayed the distribution of bacteria, the DNA of RAW264.7 cells and bacteria was stained with DAPI, and the cellular outline was marked by the white dashed circles (Fig. 5a).[64,65] Among these manipulations, the phagocytosis of macrophages from group E was more pronounced at a multiplicity of infection (MOI) of 20. The flow cytometry analysis could observe the outcome more intuitively (Fig. 5b and c). The amount of MRSA engulfed by RAW264.7 in the CIDM NCs + pro-MPCH treated group was 6.79-fold more than that of the PBS-treated group. All these data showed a consistent result with the phagocytic ability of macrophages. Besides, we confirmed that the chemicals used did not affect bacterial survival (Fig. S27†). Next, we investigated the intracellular survival of MRSA to assess the bactericidal activity of post-treatment macrophages. Based on the images of colony counting experiments, the viability of MRSA treated with CIDM NCs alone decreased slightly, which might be due to the generated ROS re-educated macrophages into the antibacterial M1 phenotype by upregulating m^{6}A methylation (Fig. 5d and e). Remarkably, group E treated with CIDM NCs + pro-MPCH displayed the strongest inhibitory capability against intracellular bacteria, and the percentage inhibition dramatically decreased

Open Access Article. Published on 28 June 2024. Downloaded on 1/18/2026 3:16:03 PM.
This article is licensed under a Creative Commons Attribution-NonCommercial 3.0 Unported Licence.

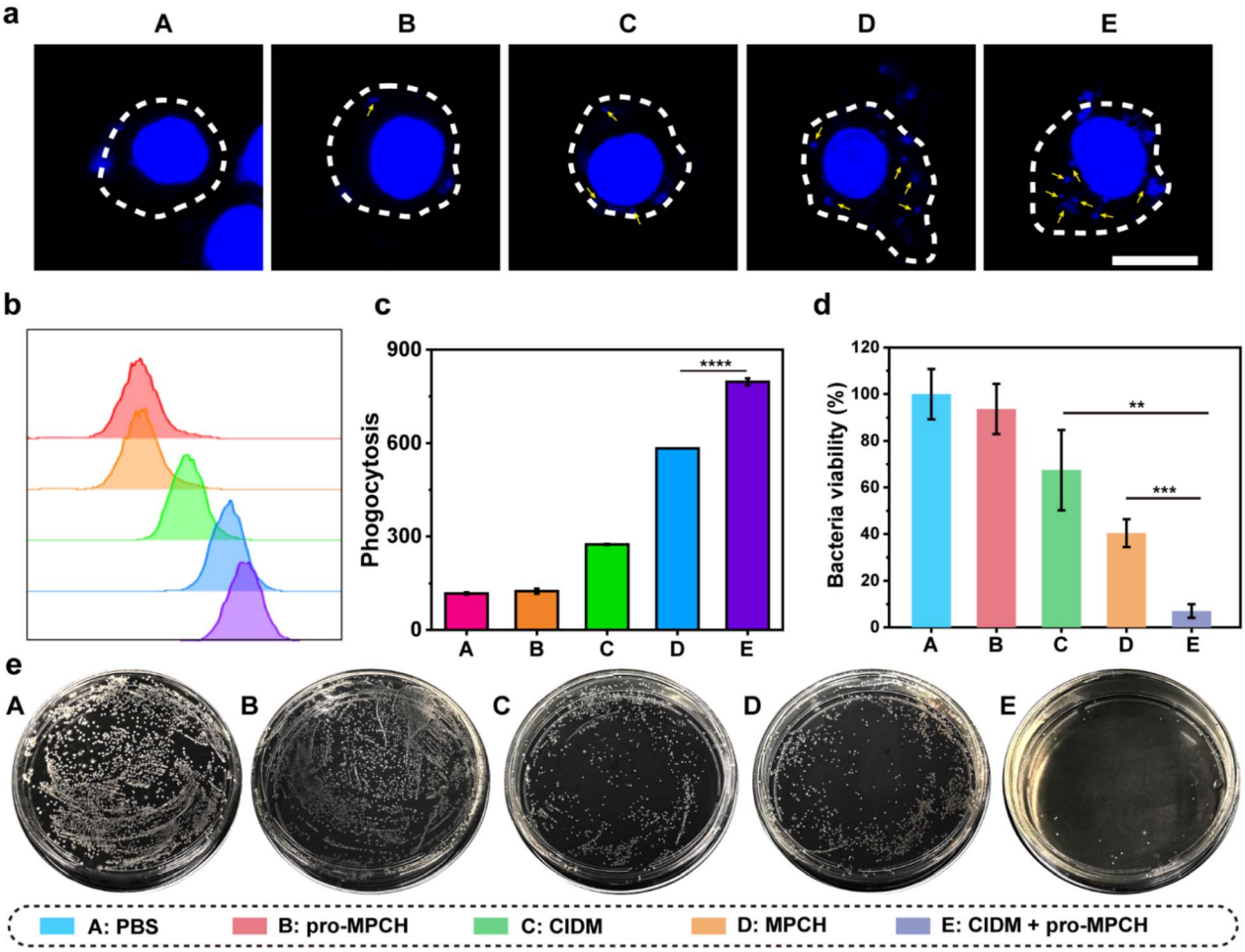

Fig. 5 (a) CLSM images, (b) flow cytometry analysis and (c) MFI of MRSA-engulfed RAW264.7 cells (MOI = 20) after treatment with A: PBS, B: pro-MPCH, C: CIDM, D: MPCH and E: CIDM + pro-MPCH, respectively. RAW264.7 cells were pre-incubated with IL-4 (25 ng mL^{-1}) for 12 h. The cellular outline is circled with a white dashed line. DAPI stained the DNA of RAW264.7 cells and bacterial cells. The small blue dots are MRSA as indicated by yellow arrows. The large blue dots are macrophage nuclei. Scale bar = 10 μm. (d) Intracellular percentage survival of MRSA in cells and (e) corresponding photographs of MRSA colonies after various pretreatments. Experimental conditions: CIDM (50 μg mL^{-1}), pro-MPCH (100 nM), 5 mM NaAsc. Data were presented as mean ± s.d. ($n = 3$). **$P < 0.01$, ***$P < 0.001$, ****$p < 0.0001$.

to 7.02% (Fig. 5d). The results identified the excellent bactericidal capacity of the bioorthogonal catalysis system. Reports demonstrated that reactive oxygen species (ROS) are a crucial component of the antimicrobial activity of macrophages. Then the secretion of ROS in macrophages after different treatments was detected. Fig. S28† confirms that macrophages generated a large number of ROS after being treated with CIDM + pro-MPCH compared to the PBS group. To further confirm that bacteria are primarily killed by re-educated macrophages *via* the production of ROS, a commonly used thiol-containing ROS scavenger *N*-acetyl cysteine (NAC) was chosen in the following experiment.[66,67] The NAC scavenges oxidants by triggering intracellular H_2S and sulfane/sulfur production.[68,69] As shown in Fig. S29,† over 80% of the bacteria survived after being treated with NAC, implying that suppressing ROS generation affected the bactericidal ability of re-educated macrophages. Consequently, the above results testified that our bioorthogonal catalysis strategy was a promising method to *in situ* regulate m^6A methylation and repolarize macrophages, minimize side effects, and eliminate intracellular bacteria.

Conclusion

In summary, we proposed and successfully constructed a bioorthogonal catalysis system, which enables controlled manipulation of m^6A modification and minimizes drug side effects. This prepared CIDM performed easy penetration and effective catalysis due to the characteristics of ultrasmall size and large specific surface area. By modifying with mannose, the well-designed nanocatalyst selectively accumulated in macrophages and activated the prodrug *in situ*, avoiding the unpredictable consequences of affecting the methylation levels in other cells. Additionally, the nanocatalyst displayed OXD-like activity further enhancing the level of m^6A methylation. *In vitro* antimicrobial results proved that controllable *in situ* m^6A methylation modulation *via* agonist activation and ROS generation could polarize macrophages into the M1-type and

© 2024 The Author(s). Published by the Royal Society of Chemistry

Open Access Article. Published on 28 June 2024. Downloaded on 1/18/2026 3:16:03 PM. This article is licensed under a Creative Commons Attribution-NonCommercial 3.0 Unported Licence.

effectively eliminate bacteria. Recently, the METTL3 inhibitor STC-15 has entered clinical trials (NCT05584111),[70] highlighting the exciting potential of regulating m^{6}A methylation in clinics. Given the desirable antimicrobial effects of the designed strategy, we think that this *in situ* modulation of RNA methylation, which enhances overall methylation levels, is meaningful and holds therapeutic potential. Although still in its infancy, we believe our bioorthogonal chemistry-controlled strategy will offer a new perspective for *in situ* controllable modulation of m^{6}A methylation.

Data availability

The data supporting this article have been included as part of the ESI.†

Author contributions

M. S. designed and conceived the experiments, implemented the experiments, analysed the data and wrote the manuscript; J. R. and X. Q. designed and conceived the experiments, supervised the study and revised the manuscript. All authors approved the final version.

Conflicts of interest

There are no conflicts to declare.

Acknowledgements

Financial support was provided by the National Key R&D Program of China (2021YFF1200700, 2021YFF1200700, and 2022YFA1205804) and National Natural Science Foundation of China (grant no. 22237006 and 21977091).

References

1 J.-M. Fustin, R. Kojima, K. Itoh, H.-Y. Chang, S. Ye, B. Zhuang, A. Oji, S. Gibo, R. Narasimamurthy, D. Virshup, G. Kurosawa, M. Doi, I. Manabe, Y. Ishihama, M. Ikawa and H. Okamura, Two Ck1δ transcripts regulated by m^{6}A methylation code for two antagonistic kinases in the control of the circadian clock, *Proc. Natl. Acad. Sci. U. S. A.*, 2018, **115**, 5980–5985.

2 B. S. Zhao, I. A. Roundtree and C. He, Post-transcriptional gene regulation by mRNA modifications, *Nat. Rev. Mol. Cell Biol.*, 2016, **18**, 31–42.

3 Q. Cui, H. Shi, P. Ye, L. Li, Q. Qu, G. Sun, G. Sun, Z. Lu, Y. Huang, C.-G. Yang, A. D. Riggs, C. He and Y. Shi, m^{6}A RNA Methylation Regulates the Self-Renewal and Tumorigenesis of Glioblastoma Stem Cells, *Cell Rep.*, 2017, **18**, 2622–2634.

4 C. Zhang, D. Samanta, H. Lu, J. W. Bullen, H. Zhang, I. Chen, X. He and G. L. Semenza, Hypoxia induces the breast cancer stem cell phenotype by HIF-dependent and ALKBH5-mediated m6A-demethylation of NANOG mRNA, *Proc. Natl. Acad. Sci. U. S. A.*, 2016, **113**, E2047.

5 S. Yang, J. Wei, Y.-H. Cui, G. Park, P. Shah, Y. Deng, A. E. Aplin, Z. Lu, S. Hwang, C. He and Y.-Y. He, m^{6}A mRNA demethylase FTO regulates melanoma tumorigenicity and response to anti-PD-1 blockade, *Nat. Commun.*, 2019, **10**, 2782.

6 L. Fabbri, A. Chakraborty, C. Robert and S. Gagner, The plasticity of mRNA translation during cancer progression and therapy resistance, *Nat. Rev. Cancer*, 2021, **21**, 558–577.

7 S. Panneerdoss, V. K. Eedunuri, P. Yadav, S. Timilsina, S. Rajamanickam, S. Viswanadhapalli, N. Abdelfattah, B. C. Onyeagucha, X. Cui, Z. Lai, T. A. Mohammad, Y. K. Gupta, T. H.-M. Huang, Y. Huang, Y. Chen and M. K. Rao, Cross-talk among writers, readers, and erasers of m^{6}A regulates cancer growth and progression, *Sci. Adv.*, 2018, **4**, eaar8263.

8 I. Barbieri and T. Kouzarides, Role of RNA modifications in cancer, *Nat. Rev. Cancer*, 2020, **20**, 303–322.

9 Y. Wang, Y. Li, M. Yue, J. Wang, S. Kumar, R. J. Wechsler-Reya, Z. Zhang, Y. Ogawa, M. Kellis, G. Duester and J. C. Zhao, N^6-methyladenosine RNA modification regulates embryonic neural stem cell self-renewal through histone modifications, *Nat. Neurosci.*, 2018, **21**, 195–206.

10 J. Wen, R. T. Lv, H. H. Ma, H. J. Shen, C. X. He, J. H. Wang, F. F. Jiao, H. Liu, P. Y. Yang, L. Tan, F. Lan, Y. J. G. N. Shi, C. He, Y. Shi and J. B. Diao, Zc3h13 Regulates Nuclear RNA m^{6}A Methylation and Mouse Embryonic Stem Cell Self-Renewal, *Mol. Cell*, 2018, **69**, 1028–1038.

11 X. Deng, Y. Qing, D. Horne, H. Huang and J. Chen, The roles and implications of RNA m^{6}A modification in cancer, *Nat. Rev. Clin. Oncol.*, 2023, **20**, 507–526.

12 H.-B. Li, J. Tong, S. Zhu, P. J. Batista, E. E. Duffy, J. Zhao, W. Bailis, G. Cao, L. Kroehling, Y. Chen, G. Wang, J. P. Broughton, Y. G. Chen, Y. Kluger, M. D. Simon, H. Y. Chang, Z. Yin and R. A. Flavell, m^{6}A mRNA methylation controls T cell homeostasis by targeting the IL-7/STAT5/SOCS pathways, *Nature*, 2017, **548**, 338–342.

13 Y. Liu, G. H. Liang, H. J. Xu, W. X. Dong, Z. Dong, Z. W. Qiu, Z. H. Zhang, F. L. Li, Y. Huang, Y. L. Li, J. Wu, S. Y. Yin, Y. W. Zhang, P. J. Guo, J. Liu, J. Z. J. Xi, P. Jiang, D. L. Han, C. G. Yang and M. M. Xu, Tumors exploit FTO-mediated regulation of glycolytic metabolism to evade immune surveillance, *Cell Metab.*, 2021, **33**, 1221–1233.

14 D. Han, J. Liu, C. Chen, L. Dong, Y. Liu, R. Chang, X. Huang, Y. Liu, J. Wang, U. Dougherty, M. B. Bissonnette, B. Shen, R. R. Weichselbaum, M. M. Xu and C. He, Anti-tumour immunity controlled through mRNA m^{6}A methylation and YTHDF1 in dendritic cells, *Nature*, 2019, **566**, 270–274.

15 Y. Liu, Z. Liu, H. Tang, Y. Shen, Z. Gong, N. Xie, X. Zhang, W. Wang, W. Kong, Y. Zhou and Y. Fu, The N^6-methyladenosine (m^{6}A)-forming enzyme METTL3 facilitates M1 macrophage polarization through the methylation of STAT1 mRNA, *Am. J. Physiol.: Cell Physiol.*, 2019, **317**, C762–C775.

16 J. Tong, X. Wang, Y. Liu, X. Ren, A. Wang, Z. Chen, J. Yao, K. Mao, T. Liu, F.-L. Meng, W. Pan, Q. Zou, J. Liu, Y. Zhou, Q. Xia, R. A. Flavell, S. Zhu and H.-B. Li, Pooled CRISPR

Open Access Article. Published on 28 June 2024. Downloaded on 1/18/2026 3:16:03 PM. This article is licensed under a Creative Commons Attribution-NonCommercial 3.0 Unported Licence.

screening identifies m^{6}A as a positive regulator of macrophage activation, *Sci. Adv.*, 2021, **7**, eabd4742.

17 Y. Liu, Y. L. You, Z. K. Lu, J. Yang, P. P. Li, L. Liu, H. N. Xu, Y. M. Niu and X. T. Cao, N^6-methyladenosine RNA modification-mediated cellular metabolism rewiring inhibits viral replication, *Science*, 2019, **365**, 1171–1176.

18 Q. You, F. Wang, R. Du, J. N. Pi, H. Y. Wang, Y. Huo, J. Y. Liu, C. Wang, J. Yu, Y. L. Yang and L. Zhu, m^{6}A Reader YTHDF1-Targeting Engineered Small Extracellular Vesicles for Gastric Cancer Therapy via Epigenetic and Immune Regulation, *Adv. Mater.*, 2023, **35**, e2204910.

19 X. M. Liu, J. Zhou, Y. H. Mao, Q. Q. Ji and S. B. Qian, Programmable RNA N^6-methyladenosine editing by CRISPR-Cas9 conjugates, *Nat. Chem. Biol.*, 2019, **15**, 865–871.

20 J. N. Wang, F. Wang, J. Ke, Z. Li, C. H. Xu, Q. Yang, X. Chen, X. Y. He, Y. He, X. G. Suo, C. Li, J. T. Yu, L. Jiang, W. J. Ni, J. Jin, M. M. Liu, W. Shao, C. Yang, Q. Gong, H. Y. Chen, J. Li, Y. G. Wu and X. M. Meng, Inhibition of METTL3 attenuates renal injury and inflammation by alleviating m^{6}A modifications via IGF2BP2-dependent mechanisms, *Sci. Transl. Med.*, 2022, **14**, eabk2709.

21 C. Wilson, P. J. Chen, Z. Miao and D. R. Liu, Programmable m^{6}A modification of cellular RNAs with a Cas13-directed methyltransferase, *Nat. Biotechnol.*, 2020, **38**, 1431–1440.

22 R. Su, L. Dong, C. Li, S. Nachtergaele, M. Wunderlich, Y. Qing, X. Deng, Y. Wang, X. Weng, C. Hu, M. Yu, J. Skibbe, Q. Dai, D. Zou, T. Wu, K. Yu, H. Weng, H. Huang, K. Ferchen, X. Qin, B. Zhang, J. Qi, A. T. Sasaki, D. R. Plas, J. E. Bradner, M. Wei, G. Marcucci, X. Jiang, J. C. Mulloy, J. Jin, C. He and J. Chen, R-2HG Exhibits Anti-tumor Activity by Targeting FTO/m^{6}A/MYC/CEBPA Signaling, *Cell*, 2018, **172**, 90–105.e123.

23 B. Chen, F. Ye, L. Yu, G. Jia, X. Huang, X. Zhang, S. Peng, K. Chen, M. Wang, S. Gong, R. Zhang, J. Yin, H. Li, Y. Yang, H. Liu, J. Zhang, H. Zhang, A. Zhang, H. Jiang, C. Luo and C.-G. Yang, Development of Cell-Active N^6-Methyladenosine RNA Demethylase FTO Inhibitor, *J. Am. Chem. Soc.*, 2012, **134**, 17963–17971.

24 H. Li, H. Wu, Q. Wang, S. Ning, S. Xu and D. Pang, Dual effects of N^6-methyladenosine on cancer progression and immunotherapy, *Mol. Ther.–Nucleic Acids*, 2021, **24**, 25–39.

25 K. X. Cao, Y. Y. Du, X. Bao, M. D. Han, R. Su, J. X. Pang, S. J. Liu, Z. Shi, F. Yan and S. H. Feng, Glutathione-Bioimprinted Nanoparticles Targeting of N^6-methyladenosine FTO Demethylase as a Strategy against Leukemic Stem Cells, *Small*, 2022, **18**, e2106558.

26 L. Lan, Y. J. Sun, X. Y. Jin, L. J. Xie, L. Liu and L. Cheng, A Light-Controllable Chemical Modulation of m^{6}A RNA Methylation, *Angew. Chem., Int. Ed.*, 2021, **60**, 18116–18121.

27 L.-J. Xie, R.-L. Wang, D. Wang, L. Liu and L. Cheng, Visible-light-mediated oxidative demethylation of N^6-methyl adenines, *Chem. Commun.*, 2017, **53**, 10734–10737.

28 L.-J. Xie, X.-T. Yang, R.-L. Wang, H.-P. Cheng, Z.-Y. Li, L. Liu, L. Mao, M. Wang and L. Cheng, Identification of Flavin Mononucleotide as a Cell-Active Artificial N^6-Methyladenosine RNA Demethylase, *Angew. Chem., Int. Ed.*, 2019, **58**, 5028–5032.

29 J. Li, S. Jia and P. R. Chen, Diels-Alder reaction-triggered bioorthogonal protein decaging in living cells, *Nat. Chem. Biol.*, 2014, **10**, 1003–1005.

30 J. A. Prescher and C. R. Bertozzi, Chemistry in living systems, *Nat. Chem. Biol.*, 2005, **1**, 13–21.

31 E. M. Sletten and C. R. Bertozzi, Bioorthogonal Chemistry: Fishing for Selectivity in a Sea of Functionality, *Angew. Chem., Int. Ed.*, 2009, **48**, 6974–6998.

32 H. Wang, M. C. Sobral, D. K. Y. Zhang, A. N. Cartwright, A. W. Li, M. O. Dellacherie, C. M. Tringides, S. T. Koshy, K. W. Wucherpfennig and D. J. Mooney, Metabolic labeling and targeted modulation of dendritic cells, *Nat. Mater.*, 2020, **19**, 1244–1252.

33 H. Wang, R. B. Wang, K. M. Cai, H. He, Y. Liu, J. Yen, Z. Y. Wang, M. Xu, Y. W. Sun, X. Zhou, Q. Yin, L. Tang, I. T. Dobrucki, L. W. Dobrucki, E. J. Chaney, S. A. Boppart, T. M. Fan, S. Lezmi, X. S. Chen, L. C. Yin and J. J. Cheng, Selective in vivo metabolic cell-labeling-mediated cancer targeting, *Nat. Chem. Biol.*, 2017, **13**, 415–424.

34 M. Tomás-Gamasa, M. Martínez-Calvo, J. R. Couceiro and J. L. Mascareñas, Transition metal catalysis in the mitochondria of living cells, *Nat. Commun.*, 2016, **7**, 12538.

35 J. Li and P. R. Chen, Development and application of bond cleavage reactions in bioorthogonal chemistry, *Nat. Chem. Biol.*, 2016, **12**, 129–137.

36 J. Geng, Y. C. A. Zhang, Q. Gao, K. Neumann, H. Dong, H. Porter, M. Potter, H. Ren, D. Argyle and M. Bradley, Switching on prodrugs using radiotherapy, *Nat. Chem.*, 2021, **13**, 805–810.

37 Z. W. Chen, H. J. Li, Y. J. Bian, Z. J. Wang, G. J. Chen, X. D. Zhang, Y. M. Miao, D. Wen, J. Q. Wang, G. Wan, Y. Zeng, P. Abdou, J. Fang, S. Li, C. J. Sun and Z. Gu, Bioorthogonal catalytic patch, *Nat. Nanotechnol.*, 2021, **16**, 933–941.

38 L. P. Liu, D. Y. Zhang, M. Johnson and N. K. Devaraj, Light-activated tetrazines enable precision live-cell bioorthogonal chemistry, *Nat. Chem.*, 2022, **14**, 1078–1085.

39 J. A. Ko, M. Wilkovitsch, J. Oh, R. H. Kohler, E. Bolli, M. J. Pittet, C. Vinegoni, D. B. Sykes, H. Mikula, R. Weissleder and J. C. T. Carlson, Spatiotemporal multiplexed immunofluorescence imaging of living cells and tissues with bioorthogonal cycling of fluorescent probes, *Nat. Biotechnol.*, 2022, **40**, 1654–1662.

40 B. Akgun and D. G. Hall, Boronic Acids as Bioorthogonal Probes for Site-Selective Labeling of Proteins, *Angew. Chem., Int. Ed.*, 2018, **57**, 13028–13044.

41 Q. Y. Wang, Y. P. Wang, J. J. Ding, C. H. Wang, X. H. Zhou, W. Q. Gao, H. W. Huang, F. Shao and Z. B. Liu, A bioorthogonal system reveals antitumour immune function of pyroptosis, *Nature*, 2020, **579**, 421–426.

42 T. Peng and H. C. Hang, Site-Specific Bioorthogonal Labeling for Fluorescence Imaging of Intracellular Proteins in Living Cells, *J. Am. Chem. Soc.*, 2016, **138**, 14423–14433.

43 J. Clavadetscher, E. Indrigo, S. V. Chankeshwara, A. Lilienkampf and M. Bradley, In-Cell Dual Drug

© 2024 The Author(s). Published by the Royal Society of Chemistry

Open Access Article. Published on 28 June 2024. Downloaded on 1/18/2026 3:16:03 PM. This article is licensed under a Creative Commons Attribution-NonCommercial 3.0 Unported Licence.

Synthesis by Cancer-Targeting Palladium Catalysts, *Angew. Chem., Int. Ed.*, 2017, **56**, 6864–6868.

44 G. Y. Tonga, Y. Jeong, B. Duncan, T. Mizuhara, R. Mout, R. Das, S. T. Kim, Y.-C. Yeh, B. Yan, S. Hou and V. M. Rotello, Supramolecular regulation of bioorthogonal catalysis in cells using nanoparticle-embedded transition metal catalysts, *Nat. Chem.*, 2015, **7**, 597–603.

45 J. J. Yang, K. Y. Yang, S. Y. Du, W. Luo, C. Wang, H. M. Liu, K. G. Liu, Z. B. Zhang, Y. F. Gao, X. Han and Y. J. Song, Bioorthogonal Reaction-Mediated Tumor-Selective Delivery of CRISPR/Cas9 System for Dual-Targeted Cancer Immunotherapy, *Angew. Chem., Int. Ed.*, 2023, **62**, e202306863.

46 Z. Liu, M. Sun, W. Zhang, J. Ren and X. Qu, Target-Specific Bioorthogonal Reactions for Precise Biomedical Applications, *Angew. Chem., Int. Ed.*, 2023, **62**, e202308396.

47 M. Y. Sun, Z. W. Liu, L. Wu, J. Yang, J. S. Ren and X. G. Qu, Bioorthogonal-Activated In Situ Vaccine Mediated by a COF-Based Catalytic Platform for Potent Cancer Immunotherapy, *J. Am. Chem. Soc.*, 2023, **145**, 5330–5341.

48 C. C. Huang, C. Q. Zhao, Q. Q. Deng, H. C. Zhang, J. S. Ren, D. Q. Yu and X. G. Qu, Hydrogen-bonded organic framework-based bioorthogonal catalysis prevents drug metabolic inactivation, *Nat. Catal.*, 2023, **6**, 729–739.

49 S. Selberg, D. Blokhina, M. Aatonen, P. Koivisto, A. Siltanen, E. Mervaala, E. Kankuri and M. Karelson, Discovery of Small Molecules that Activate RNA Methylation through Cooperative Binding to the METTL3-14-WTAP Complex Active Site, *Cell Rep.*, 2019, **26**, 3762–3771.

50 F. Yu, J. B. Wei, X. L. Cui, C. J. Yu, W. Ni, J. Bungert, L. Z. Wu, C. A. He and Z. J. Qian, Post-translational modification of RNA m^6A demethylase ALKBH5 regulates ROS-induced DNA damage response, *Nucleic Acids Res.*, 2021, **49**, 5779–5797.

51 F. Ruan, J. Zeng, H. Yin, S. Jiang, X. Cao, N. Zheng, C. Han, C. Zhang, Z. Zuo and C. He, RNA m^6A Modification Alteration by Black Phosphorus Quantum Dots Regulates Cell Ferroptosis: Implications for Nanotoxicological Assessment, *Small Methods*, 2021, **5**, e2001045.

52 F. Ruan, C. Liu, Y. Wang, X. Cao, Z. Tang, J. Xu, J. Zeng, H. Yin, N. Zheng, C. Yang, Z. Zuo and C. He, Role of RNA m^6A modification in titanium dioxide nanoparticle-induced acute pulmonary injury: An in vitro and in vivo study, *Environ. Pollut.*, 2022, **311**, 119986.

53 Q. Gao, J. Zhang, C. Chen, M. Chen, P. Sun, W. Du, S. Zhang, Y. Liu, R. Zhang, M. Bai, C. Fan, J. Wu, T. Men and X. Jiang, In Situ Mannosylated Nanotrinity-Mediated Macrophage Remodeling Combats Candida albicans Infection, *ACS Nano*, 2020, **14**, 3980–3990.

54 M. Benoit, B. t. Desnues and J.-L. Mege, Macrophage Polarization in Bacterial Infections, *J. Immunol.*, 2008, **181**, 3733–3739.

55 S. Wan, F. Gándara, A. Asano, H. Furukawa, A. Saeki, S. K. Dey, L. Liao, M. W. Ambrogio, Y. Y. Botros, X. Duan, S. Seki, J. F. Stoddart and O. M. Yaghi, Covalent Organic Frameworks with High Charge Carrier Mobility, *Chem. Mater.*, 2011, **23**, 4094–4097.

56 Y. Zhang, L. Zhang, Z. Wang, F. Wang, L. Kang, F. Cao, K. Dong, J. Ren and X. Qu, Renal-clearable ultrasmall covalent organic framework nanodots as photodynamic agents for effective cancer therapy, *Biomaterials*, 2019, **223**, 119462.

57 N. Zion, D. A. Cullen, P. Zelenay and L. Elbaz, Heat-Treated Aerogel as a Catalyst for the Oxygen Reduction Reaction, *Angew Chem., Int. Ed.*, 2020, **59**, 2483–2489.

58 P. K. Sasmal, S. Carregal-Romero, A. A. Han, C. N. Streu, Z. Lin, K. Namikawa, S. L. Elliott, R. W. Koster, W. J. Parak and E. Meggers, Catalytic azide reduction in biological environments, *Chembiochem*, 2012, **13**, 1116–1120.

59 W. Feng, G. Li, X. Kang, R. Wang, F. Liu, D. Zhao, H. Li, F. Bu, Y. Yu, T. F. Moriarty, Q. Ren and X. Wang, Cascade-Targeting Poly(amino acid) Nanoparticles Eliminate Intracellular Bacteria via On-Site Antibiotic Delivery, *Adv. Mater.*, 2022, 2109789.

60 R. Huang, C.-H. Li, R. Cao-Milán, L. D. He, J. M. Makabenta, X. Zhang, E. Yu and V. M. Rotello, Polymer-Based Bioorthogonal Nanocatalysts for the Treatment of Bacterial Biofilms, *J. Am. Chem. Soc.*, 2020, **142**, 10723–10729.

61 Y. Sang, Q. Deng, F. Cao, Z. Liu, Y. You, H. Liu, J. Ren and X. Qu, Remodeling Macrophages by an Iron Nanotrap for Tumor Growth Suppression, *ACS Nano*, 2021, **15**, 19298–19309.

62 T. Lawrence and G. Natoli, Transcriptional regulation of macrophage polarization: enabling diversity with identity, *Nat. Rev. Immunol.*, 2011, **11**, 750–761.

63 P. Wang, B. Wu, M. Li, Y. Song, C. Chen, G. Feng, D. Mao, F. Hu and B. Liu, Lysosome-Targeting Aggregation-Induced Emission Nanoparticle Enables Adoptive Macrophage Transfer-Based Precise Therapy of Bacterial Infections, *ACS Nano*, 2023, **17**, 10365–10375.

64 G. Qi, F. Hu, L. Shi, M. Wu and B. Liu, An AIEgen-Peptide Conjugate as a Phototheranostic Agent for Phagosome-Entrapped Bacteria, *Angew. Chem., Int. Ed.*, 2019, **58**, 16229–16235.

65 M. Wu, W. Wu, Y. Duan, X. Liu, M. Wang, C. U. Phan, G. Qi, G. Tang and B. Liu, HClO-Activated Fluorescence and Photosensitization from an AIE Nanoprobe for Image-Guided Bacterial Ablation in Phagocytes, *Adv. Mater.*, 2020, **32**, e2005222.

66 Y. Zheng, D. T. Miyamoto, B. S. Wittner, J. P. Sullivan, N. Aceto, N. V. Jordan, M. Yu, N. M. Karabacak, V. Comaills, R. Morris, R. Desai, N. Desai, E. Emmons, J. D. Milner, R. J. Lee, C.-L. Wu, L. V. Sequist, W. Haas, D. T. Ting, M. Toner, S. Ramaswamy, S. Maheswaran and D. A. Haber, Expression of β-globin by cancer cells promotes cell survival during blood-borne dissemination, *Nat. Commun.*, 2017, **8**, 14344.

67 L. Xu, X. Wang, W. Wang, M. Sun, W. J. Choi, J.-Y. Kim, C. Hao, S. Li, A. Qu, M. Lu, X. Wu, F. M. Colombari, W. R. Gomes, A. L. Blanco, A. F. de Moura, X. Guo, H. Kuang, N. A. Kotov and C. Xu, Enantiomer-dependent immunological response to chiral nanoparticles, *Nature*, 2022, **601**, 366–373.

Open Access Article. Published on 28 June 2024. Downloaded on 1/18/2026 3:16:03 PM.
This article is licensed under a Creative Commons Attribution-NonCommercial 3.0 Unported Licence.

68 M. Herb and M. Schramm, Functions of ROS in Macrophages and Antimicrobial Immunity, *Antioxidants*, 2021, **10**, 313.

69 Z. Zhang, R. Dalan, Z. Hu, J.-W. Wang, N. W. Chew, K.-K. Poh, R.-S. Tan, T. W. Soong, Y. Dai, L. Ye and X. Chen, Reactive Oxygen Species Scavenging Nanomedicine for the Treatment of Ischemic Heart Disease, *Adv. Mater.*, 2022, **34**, 2202169.

70 E. Yankova, W. Blackaby, M. Albertella, J. Rak, E. De Braekeleer, G. Tsagkogeorga, E. S. Pilka, D. Aspris, D. Leggate, A. G. Hendrick, N. A. Webster, B. Andrews, R. Fosbeary, P. Guest, N. Irigoyen, M. Eleftheriou, M. Gozdecka, J. M. L. Dias, A. J. Bannister, B. Vick, I. Jeremias, G. S. Vassiliou, O. Rausch, K. Tzelepis and T. Kouzarides, Small-molecule inhibition of METTL3 as a strategy against myeloid leukaemia, *Nature*, 2021, **593**, 597–601.

© 2024 The Author(s). Published by the Royal Society of Chemistry